Characterization of Lower and Middle Pleistocene tephra beds in the southern plains of western Canada

John A. Westgate[1*], Nancy D. Naeser[2,1], René W. Barendregt[3], Nicholas J.G. Pearce[4,5]

[1] Department of Earth Sciences, University of Toronto, Toronto, Ontario, M5S 3B1 Canada

[2] United States Geological Survey, Florence Bascom Geoscience Center, 926A National Center, Reston, Virginia, 20192 USA

[3] Department of Geography and Environment, University of Lethbridge, Lethbridge, Alberta, T1K 3M4 Canada

[4] Department of Geography and Earth Sciences, Aberystwyth University, Wales, SY23 3DB, UK

[5] Dipartimento di Scienze, Biologiche, Geologiche e Ambientali, Università di Bologna, 40126, Italia

westgate@es.utoronto.ca

naeser@cox.net

barendregt@uleth.ca

njp@aber.ac.uk

Competing interests: The authors declare there are no competing interests.

Funding: This research was supported by the Natural Sciences and Engineering Research Council of Canada

Contributors' statement:

JAW: Conceived project, fieldwork, some of the fission-track dating and paleomagnetism, major-element analyses, literature, wrote most of paper. NDN: Fission-track dating and part of text. RWB: Most of the paleomagnetism, fieldwork, and part of text. NJGP: Trace-element analyses and their interpretation and related part of the text.

*Corresponding author

Email address: westgate@es.utoronto.ca

Fax number: 416-978-3938

Telephone number: 416-488-6838

Abstract

Wellsch Valley tephra, near Swift Current, southwestern Saskatchewan, and Galt Island tephra, near Medicine Hat, southeastern Alberta, have been referenced in the literature since the 1970s, but little is available on their physical and chemical attributes – necessary information if they are to be recognized elsewhere. This study seeks to remedy this situation. Both have a calc-alkaline rhyolitic composition with hornblende, biotite, plagioclase, pyroxene, and Fe-Ti oxides being dominant. They have a similar composition but are not the same. Wellsch Valley tephra has a glass fission-track age of 0.75 ± 0.05 Ma, a reversed magnetic polarity, and was deposited at the close of the Matuyama Chron. Galt Island tephra has an age of 0.49 ± 0.05 Ma, a normal magnetic polarity, and was deposited during the early Brunhes Chron. Rich fossil vertebrate faunas occur in sediments close to them. Major- and trace-element concentrations in their glass shards indicate a source in the Cascade Range of the Pacific Northwest, USA, but differences in trace-element ratios suggest they are not consanguineous.

Key words: tephra, glass shards, fission-track dating, paleomagnetism, major and trace elements, western Canada

Introduction

Southwestern Canada has a rich record of till deposits interbedded in places with stratified sediments. Sediments deposited in non-glacial environments locally occur beneath this glacial succession, and they, in turn, sit on Cretaceous bedrock (Westgate 1968, Stalker and Churcher 1972, Whitaker and Christiansen 1972, Barendregt et al. 1998). The relative age of these Quaternary deposits is well established through surface and borehole studies, but numerical ages are scarce. Tephra beds are rare in the southern plains of western Canada due to the distant location of volcanoes, which are mostly in the western USA, but when present they offer excellent opportunities for improved age control on the closely associated deposits as well as the prospect of reliable correlation to deposits elsewhere. Eruptions that have shed tephra across this region include Mazama tephra from Crater Lake, Oregon (~ 7 ka, Buckland et al. 2020), Glacier Peak tephra from Glacier Peak, Washington (11 – 13 ka, Westgate and Evans 1978), Wascana Creek tephra (Lava Creek B) from Yellowstone caldera, Wyoming (0.63 Ma, Westgate et al. 1977), and Bandelier Tuff from Valles caldera, New Mexico (1.2 Ma, Westgate et al. 2019).

Since the 1970s, two tephra beds in the southwestern plains of western Canada have been known to exist but their intrinsic properties have so far received scant study. They are the Wellsch Valley tephra (WVt, UA115), situated about 40 km north of Swift Current, Saskatchewan, and Galt Island tephra (Gt, UA117), recognized at a site 10 km northwest of Medicine Hat, Alberta (Fig. 1). Both tephra beds are exposed in bluffs along the South Saskatchewan River (Fig. 2). The purpose of this communication is to describe their lithostratigraphic setting, physical and chemical attributes, age, and paleomagnetic properties so that other workers will be able to recognize them should they occur in their tephra studies elsewhere. Old and new data are brought together to provide a comprehensive characterization. Comments are also included on the likely source of these two tephra beds.

Previous work

The Wellsch Valley site, known as the "Jaw Face" section, was first described by Stalker and Churcher (1972). The top part of the section consists of glacial deposits, tills and fluvial sand and gravel, below which are fine-grained stratified sediments that contain the Wellsch Valley tephra. A more detailed lithostratigraphy is given in Churcher and Stalker (unpublished manuscript, Geology and vertebrate paleontology of the Wellsch Valley site, Saskatchewan, 1988) but illustrated in Barendregt (1991) and Barendregt et al. (1998).

Numerous vertebrate fossils have been found in the stratified sediments below WVt (Westgate et al. 1978, Churcher 1984). An early Quaternary age is suggested by the presence of late Blancan – Irvingtonian forms, using the North American Land Mammal Age (NALMA) terminology.

The first paleomagnetic study of the Jaw Face section is that done by Foster and Stalker (1976). They showed that WVt has a reversed magnetic polarity. In addition, two intervals of normal magnetic polarity were identified below WVt, the lower one being correlated to the Olduvai Subchron with an age of ~ 1.8 Ma. On the other hand, Barendregt et al. (1991) found no good evidence for normal polarity intervals below WVt despite very detailed sampling. They attributed the normal polarity intervals below WVt, described by Foster and Stalker (1976), as likely due to incompletely resolved magnetizations—that is, some overprint was still present. Thus, according to Barendregt et al. (1991), the entire section at and below WVt is reversed whereas the magnetic polarity is normal above WVt. This polarity sequence holds true for the later detailed paleomagnetic study of Barendregt et al. (1998), which included samples taken from borehole cores drilled at nearby sites. In this case even the tills above WVt were sampled and found to have a normal magnetic polarity.

An analysis of the rhyolitic glass shards of WVt by Westgate is given in Stalker and Churcher (1972), and a glass fission-track age of 0.69 Ma was noted in a talk by Westgate et al. (1978), but this age and its supporting information was not published. This age determination is a minimum estimate because the age had not been corrected for partial track fading.

A. MacS Stalker (Geological Survey of Canada) discovered the Galt Island section in the 1970s, including the Galt Island tephra (Gt) and the rich assemblage of vertebrate fossils just above it, both near the base of the Quaternary sediments, but little is available in print. C. S. Churcher (University of Toronto) studied the vertebrate fossils and considered them to be of Rancholabrean age (Westgate et al. 1978). Two ^{14}C ages of 37,900 ± 1100 (GSC-1442) and 38,700 ± 1100 (GSC-1442-2) years B.P. (Lowdon and Blake 1975), just above the fossiliferous zone, led to the view that the vertebrate fauna was of mid-Wisconsin age (Stalker 1977), but an uncorrected glass fission-track age of 0.43 Ma (Westgate et al. 1978) for the Gt indicates it is much older but still consistent with the NALMA designation. These lowermost Quaternary deposits at the Galt Island section have a normal magnetic polarity (Barendregt 1984) and so belong to the Brunhes Chron, consonant with the age of the vertebrate fossils and fission-track age of Gt.

We emphasize that the uncorrected fission-track ages for WVt and Gt along with their supporting counting statistics were mentioned in the 1978 Geological Society of America talk (Westgate et al. 1978) but never published.

Methods

Sample preparation for major- and trace-element analysis involved dry sieving the bulk tephra to obtain the coarsest size fraction that contained abundant glass shards. The 0.125 - 0.088 mm fraction was used for the Wellsch Valley tephra (WVt) and the 0.088 - 0.063 mm fraction for the finer-grained Galt Island tephra (Gt). Each sample was cleaned ultrasonically for 10 minutes, dried under a lamp, and sieved again to concentrate the coarsest material. Minerals were separated from glass, and pumiceous glass from platy and bubble-wall glass shards, using a Frantz Isodynamic Magnetic Separator. The platy and bubble-wall glass shards of each tephra bed were then mounted in an epoxy resin block and polished for analysis.

Both size fractions were used to determine the fission-track age of WVt, but, of necessity, only the finer size fraction was used for Gt. Glass shards were concentrated by use of heavy liquids, a practice followed in the 1970s, when the samples were processed for fission-track analysis (Smith and Westgate 1968). Pumice fragments were floated off first and then a heavier fraction, in which mineral grains and composites were concentrated, was removed. The specific gravity of the liquid was adjusted empirically to obtain a separate rich in platy and bubble-wall glass shards including pumice fragments of low vesicularity. Glass shards from each sample were then mounted in epoxy resin on glass slides, left to harden for several days, polished, and etched in HF to reveal the fission tracks.

The major-element composition of the glass shards was determined using a Cameca SX50 microprobe at the University of Toronto. Analyses were performed with 15 kV accelerating voltage, 6 nA beam current, and a 10 μm defocused beam. Standardization was achieved through mineral and glass standards. The reference glass used in this study to monitor the calibration is the Old Crow tephra glass (Westgate et al. 1985). All glass analyses were recast to 100 wt%

anhydrous with the difference from 100 wt% being considered as H_2O_d, although it is recognized that very small concentrations of elements such as P, F, and S are likely present. The EPMA software removes low or negative concentrations, which here results in a few MnO analyses being unreported, and, like the missing minor elements this will have a very small effect on analytical totals for a small number of analyses (see Supplementary Table 1). The Fe-Ti oxide mineral analyses were done on an ARL "EMX" microprobe fitted with an Ortec Si(Li) detector, which was operated at 20 kV accelerating voltage with a beam current set to give 3000 counts/s on willemite, sample current ~ 20 nA, and counting time 100 s. Data reduction was by a modified version of PESTRIPS. Standards used were the Ødergarden ilmenite and the Elba hematite.

Trace-element analyses of glass shards were performed at Aberystwyth University using a Coherent GeoLas ArF 193 nm Excimer laser ablation system operating at a fluence of 10 J cm^{-2} and a repetition rate of 5 Hz. Analyses were all performed using 20 μm ablation craters. Spectra were acquired for 24 seconds on a Thermo Finnegan Element 2 sector field ICP-MS. The minor ^{29}Si isotope was used as the internal standard (taking the anhydrous, normalized SiO_2 concentration determined by EPMA) and calibration was achieved against the NIST SRM 612 certified reference glass, using concentrations from Pearce et al. (1997). A fractionation factor was applied to the analyses to account for matrix effects which cause differences in the removal of individual elements from the unknowns when compared to the reference glasses, these resulting largely from differences in the degree of polymerization (related to the major element composition) of the glasses (Pearce et al. 2011). The fractionation factor was determined from many separate analytical sessions analyzing the MPI-DING ATHO-G rhyolitic reference glass and performed over several years. Sample data were filtered to remove analyses which had clearly ablated phenocryst phases to leave only analyses of the pure glass phase. Outlying analyses were also removed from the calculations of averages, these resulting from random analytical noise (a "spike") either in the analyte signal, resulting in a high concentration, or in the blank, giving low or negative concentrations. No elements in the analysed samples were routinely below the calculated 3-sigma detection limits (see Supplementary Table 2). Details of analytical and data filtering methods, as well as ICP-MS and laser operating conditions, are given in Pearce et al. (2011, 2014) and Pearce (2014), and references therein. The MPI-DING reference glass ATHO-G was analysed as an unknown under the same operating conditions at the same time with data presented in Table 1 and Table S2. Analytical precision is typically between ±5-10%, and accuracy is typically around ±5%, when compared with the published concentrations for ATHO-G (Jochum and Stoll 2008).

The ages of WVt and Gt were determined using the glass fission-track method. The spontaneous and induced (by irradiation) track densities in glass shards separated from the tephra samples were determined using the population-subtraction method (Westgate 2015). The area of glass was determined by the point-counting technique (Naeser et al. 1982). The samples were initially dated in the 1970s. Later, the data were used to recalculate the ages using the zeta age calibration method (Hurford and Green 1983, Wagner and Van den Haute 1992), with a zeta factor of 315 ± 3. The ages of WVt and Gt have been corrected for partial fading of spontaneous tracks, either by using the diameter correction method (DCFT) (Sandhu and Westgate 1995) or by heating the glass shards for 1 hr at 200°C (Naeser and Naeser 1988). Accuracy of the age determinations was monitored by dating Moldavite tektite standard glass (Schmieder et al. 2018) as an unknown.

Determination of the paleomagnetic properties of WVt and Gt required the collection of oriented samples of sediment in plastic cubes with 2 cm sides. These cubes were gently tapped into the sediment with a rubber mallet and were held firmly in position against the vertical face of the exposure by a small, aluminium holder containing a shallow, recessed area into which the cube was snugly fitted. In the unpublished study by Westgate in the 1970s, samples at the Jaw Face section were collected about 10 cm apart at each stratigraphic level. In a later study by Barendregt (1984) sampling was carried out at a nearby site (15 m east of the Jaw Face section, the original discovery site) and involved a more extensive excavation of the sediment sequence. Here, 100 single samples were collected in a vertical string, approximately 6-8 cm apart. At the Gt outcrop 8 samples were collected from each of 15 horizons, and each horizon was approximately 10 cm apart.

For the study by Westgate at the Wellsch Valley section, remanence measurements were made at the University of Toronto using a cryogenic magnetometer built by Develco Corporation and the alternating field demagnetization was performed with an instrument made by Schonstedt Corporation. Most of the samples were demagnetized up to a peak field of 5 mT but two samples below WVt were demagnetized up to a peak field of 10 mT. Some detailed stepwise demagnetizations were carried to higher fields to determine the stability of the remanence. In the study by Barendregt at Wellsch Valley and Galt Island, samples were measured using a 2G cryogenic magnetometer at University of California, Davis. Samples were demagnetized in alternating fields of 10, 30, 50, and 70 mT.

Lithostratigraphy

Wellsch Valley tephra (UA115) is exposed on the eastern side of Wellsch Valley, which leads into the South Saskatchewan River (Fig. 2). The section is about 16 m thick. The tephra bed is situated about 10 m above the top of the Cretaceous bedrock and separates a younger sequence of sediments formed in glacial environments – mainly tills and proglacial lake deposits – from a variety of fine-grained, fossiliferous sediments that accumulated in non-glacial environments (Fig. 3) – specifically, fluvial, lacustrine, and aeolian deposits probably laid down in a floodplain setting in which lakes and streams were likely shallow and intermittent (Churcher and Stalker, unpublished manuscript mentioned in Barendregt et al. 1998). The lowermost unit, immediately above bedrock, is distinctive. It consists mainly of reworked bedrock with scattered stone beds, angular fragments of ironstone and petrified wood along with rounded pebbles of quartzite and sandstone (Barendregt et al. 1991). Sediments below the glacial deposits and above bedrock belong to the Empress Group, as defined by Whitaker and Christiansen (1972).

Wellsch Valley tephra is laterally discontinuous across the section and is about 10 cm thick, but can be thicker due to reworking, in part by burrowing rodents and admixture with silt, which is probably loess. It fell on a desiccated surface with tephra filling mudcracks (Fig. 4). Based on four analyses of almost pure tephra, WVt has 5 wt% sand-sized tephra, 90 wt% silt, and 5 wt% clay-sized tephra. The median grain-size is 5.25 φ units, the inclusive graphic standard deviation (σ_I) (Folk 1961) is 1.06 φ units, and the size distributions are shown in Figure 5.

Galt Island tephra (UA117) is exposed near the base of the Quaternary sedimentary sequence on the northern bluff of the South Saskatchewan River, near Redcliff, Alberta (Figs. 1, and 2). It occurs immediately above gravels (Fig. 6) that consist mainly of rounded quartzite pebbles whose provenance is to the west in the region of the Rocky Mountains. Stones from the Canadian Shield are absent so that these gravels are regarded as preglacial in the sense that they were deposited prior to the initial incursion of the Laurentide glacier into southeastern Alberta. Galt Island tephra (Gt) is impure, occurs mostly as blebs in the fine-grained sediment, and is traceable laterally for about 20 meters. A sample with only minor contamination has a median grain size of 5.8 φ units, and a σ_I value of 2.12 φ units, which makes it finer grained and more poorly sorted than WVt. The sand, silt, and clay-sized tephra wt% values are 5: 80: 15, respectively (Fig. 5). Alluvial sand, silt, and clay just above Gt are rich in vertebrate fossils (Westgate et al. 1978) and plant remains, including wood fragments that yielded ^{14}C ages of 37,900 ± 1100 (GSA-1442) and 38,700 ± 1100 (GSC-1442-2) years B.P. (Fig. 6).

A thick sequence of laminated silt and clay is the dominant Quaternary sedimentary unit of the section. These are lacustrine deposits, the upper part of which likely accumulated in a proglacial lake, and, with the succeeding fluvial gravels, heralds the progressive encroachment of the Laurentide Ice Sheet into southeastern Alberta, when the till was deposited.

Composition

Wellsch Valley tephra and Gt have similar compositions but not the same. Minerals in WVt are hornblende, plagioclase, magnetite, ilmenite, and biotite, with minor or trace amounts of basaltic hornblende, orthopyroxene, clinopyroxene, apatite, and zircon. Orthopyroxene is the dominant mineral in Gt, which also contains plagioclase, magnetite, ilmenite, hornblende, biotite, clinopyroxene, apatite, and zircon.

Both tephra beds are classified as calc-alkaline rhyolites based on their glass composition (Le Maitre et al. 2002), although the primary mineral grains are sufficiently abundant that the bulk composition of WVt is dacitic. Galt Island tephra has higher SiO_2 and lower Al_2O_3 than WVt, but concentrations of other major elements are broadly similar (Tables 1 and S1). The major-element bivariate plots in Figure 7 show WVt glass analyses to cluster closely together in contrast to Gt, which has a larger range in CaO and FeO_t concentrations. The Fe-Ti oxides in the two tephra beds also have similar compositions (Table 2). The trace-element compositions of these two tephra deposits show some significant differences (see Figure 8 and Tables 1 and S2), with particular differences in Rb, Zr, Nb, and Th, sufficient to discriminate them. Strontium in Gt has a larger range (with lower concentrations) than WVt, mirroring the variation in CaO. Because of the variation in some incompatible element concentrations, their ratios differ between Gt and WVt, with WVt having higher Nb/La (and Nb/other REE), Nb/Th, Y/Zr, and Ba/Hf ratios.

A chondrite-normalized REE plot shows similar overall average REE concentrations (Fig. 8) although Gt has higher MREE and a more pronounced negative Eu anomaly than WVt. The chondrite-normalized incompatible element spidergram (Thompson et al. 1982) in Figure 8 shows the typical depletion of Nb and Ta associated with subduction-related volcanism (Pearce 1982), with notable depletion of Ti and Sr from extraction of Fe-Ti oxides and plagioclase during magmatic evolution. Whilst these profiles are similar, the differences in Zr between the two tephra beds noted are evident. In addition, granite source discrimination (Pearce et al. 1984) based on comparisons of (Y+Nb) vs Rb, (Y+Ta) vs Rb, and Yb vs Ta (data are available in Table S2) all indicate a volcanic arc source for these magmas.

Glass fission-track ages, paleomagnetism, and source

The age of WVt was determined using the fission-track method applied to its glass shards (Westgate 2015). The results are given in Table 3. Three age estimates were determined, two in which correction for partial track fading (PTF) was achieved by the DCFT method (Sandhu and Westgate 1995), and another in which a heat treatment of 200° C for 1 hr was applied to correct for PTF. The weighted mean age of WVt is 0.75 ± 0.05 Ma.

Galt Island tephra was dated twice, and the ages corrected by the DCFT approach. In both cases, the correction factor was not determined directly by measuring the diameter of the fission tracks; instead, a value of 1.218 ± 0.04 was used for D_i/D_s based on the average D_i/D_s value from 50 determinations on glass shards from 38 different Cenozoic tephra beds (Westgate et al. 2014) (Table 3). This value for D_i/D_s is very close to that determined for WVt. The weighted mean age of Gt is 0.49 ± 0.05 Ma, which is consistent with the presence of a Rancholabrean vertebrate assemblage just above it (Westgate et al. 1978).

Paleomagnetic measurements on sediments above and below WVt were carried out in 1978 by Westgate to determine whether the age determination on WVt is consistent with the geomagnetic polarity timescale. Oriented samples were collected at 10-cm intervals from just below the tephra bed to 2.5 m above it (Fig. 9A). The inclination of remanent magnetization is positive (normal polarity) above WVt but negative (reversed polarity) at and below the tephra bed (Table 4). Given the age of 0.75 ± 0.05 Ma for WVt, this polarity change must represent the transition from the Matuyama Chron to the Brunhes Chron, dated at 783.4 ± 0.6 ka (Mark et al. 2017). A more detailed paleomagnetic study was carried out by Barendregt (1984) on a nearby site. The inclination profile (Fig. 9B) also indicates a change from reversed to normal polarity at the top of WVt.

The paleomagnetic study of the section containing Gt, near Redcliff, Alberta, was done by Barendregt (1984), who found the entire sedimentary sequence above the basal gravels to have a normal magnetic polarity, consistent with Gt belonging to the Brunhes Chron (Fig. 10).

Wellsch Valley tephra and Galt Island tephra have very similar compositions, both in terms of major and trace elements (Fig. 8, Tables 1, 2, S1, and S2). However, the differences in incompatible element ratios suggest they are either not sourced from the same volcano or are sourced from different eruptive cycles (involving magma recharge) if the source is the same; that is, from a volcanic field where eruption cycles can be spaced over long periods of time. The pronounced Nb – Ta trough in the spidergram (Fig. 8) indicates that their parental magmas formed in a continental-margin, subduction environment, which agrees with them occupying the compositional space delineated by tephra beds from vents in the Cascade Range of the Pacific Northwest (Fig. 7). It follows that the provenance of WVt and Gt most likely lies in the Cascade Range.

Conclusion

This study on the Wellsch Valley tephra and Galt Island tephra beds in the southern plains of western Canada is a blend of old and new work, although definition of their intrinsic properties is mostly new information. The resultant comprehensive characterization now permits their ready recognition elsewhere. Both tephra beds have a calc-alkaline rhyolitic composition and occur in sediments sandwiched between glacial and non-glacial deposits, which in turn rest on Cretaceous bedrock. They have a similar composition but are not the same. Wellsch Valley tephra has a glass fission-track age of is 0.75 ± 0.05 Ma, a reversed magnetic polarity, and was deposited at the close of the Matuyama Chron; according to the stratigraphic classification of Pillans and Gibbard (2012), it has an Early Pleistocene age. Galt Island tephra has an age of 0.49 ± 0.05 Ma, a normal magnetic polarity, and was deposited during the Brunhes Chron; it has a Middle Pleistocene age. Both tephra beds have associated sediments rich in fossil vertebrate faunas. Major- and trace-element concentrations in their glass shards point to a volcanic arc source in the Cascade Range of the Pacific Northwest, USA and Canada, but the difference in incompatible element ratios in particular indicates these two tephra deposits were not derived from the same magma batch and therefore probably not from the same volcano, although it does not deny a common volcanic field that experienced several distinct eruptive cycles.

Acknowledgements

This research was made possible by funds received from the Natural Sciences and Engineering Research Council of Canada. Dr. A. MacS. Stalker, Geological Survey of Canada, introduced JW to the Wellsch Valley and Galt Island tephra beds, showed him the critical geologic sections, and provided useful information on the geologic setting of the two tephra beds. The paleomagnetic analyses were done in the late 1970s under the supervision of G. William Pearce, University of Toronto, and in the 1980s under the supervision of Ken Verosub at the University of California, Davis. Then later, more detailed studies of sites near the Wellsch Valley (Jaw Face) site and other relevant sites in southern Saskatchewan, were done at the Paleomagnetism and Petrophysics Laboratory, Geological Survey of Canada - Pacific, Sidney, British Columbia, Canada with the help of Ted Irving, Judith Baker, and Randy Enkin. We thank Mary Stalker for her efforts in trying to locate a photograph of the Galt Island tephra, efforts that proved to be unsuccessful. We thank Rob Stamm for his help in guiding the manuscript through the U.S. Geological Survey Bureau approval process. Finally, we thank Stephen Kuehn, Lucy Edwards, an anonymous reviewer, and the Editors (J. Brendan Murphy and Luke Beranek) for their comments which improved the clarity of the paper. Any use of trade, firm, or product names is for descriptive purposes only and does not imply endorsement by the U.S. Government.

References

Barendregt, R.W. 1984. Correlation of Quaternary chronologies using paleomagnetism – Examples from southern Alberta and Saskatchewan. *In* Correlation of Quaternary chronologies. *Edited by* W.C. Mahaney. Geo Books, Norwich, England. pp. 59-71.

Barendregt, R.W., Thomas, F.F., Irving, E., Baker, J., Stalker, A. MacS., and Churcher, C.S. 1991. Stratigraphy and paleomagnetism of the Jaw Face section, Wellsch Valley site, Saskatchewan. Canadian Journal of Earth Sciences, **28**: 1353-1364.

Barendregt, R.W., Irving, E., Christiansen, E.A., Sauer, E.K., and Schreiner, B.T. 1998. Stratigraphy and paleomagnetism of Late Pliocene and Pleistocene sediments in the Wellsch Valley and Swift Creek areas, southwestern Saskatchewan, Canada. Canadian Journal of Earth Sciences, **35**: 1347-1361.

Buckland, H.M., Cashman, K.V., Engwell, S.L., and Rust, A.C. 2020. Sources of uncertainty in the Mazama isopachs and the implications for interpreting distal tephra deposits from large eruptions. Bulletin of Volcanology, https://doi.org/10.1007/s00445-020-1362-1

Carmichael, I.S.E. 1967. The iron-titanium oxides of salic volcanic rocks and their associated ferromagnesian silicates. Contributions to Mineralogy and Petrology, **14**: 36-64.

Carpenter, B.S., and Reimer, G.M. 1974. Standard reference materials: calibrated glass standards for fission track use. National Bureau of Standards Special Publication 260-49, 16 p.

Churcher, C.S. 1984. Faunal correlations of Pleistocene deposits in western Canada. *In* Correlation of Quaternary chronologies. *Edited by* W.C. Mahaney. Geo Books, Norwich, England. pp. 145-158.

Folk, R.L. 1961. Petrology of sedimentary rocks. Hemphill's, Austin, Texas, 154 p.

Foster, J.H., and Stalker, A. MacS. 1976. Paleomagnetic stratigraphy of the Wellsch Valley site, Saskatchewan. Report of Activities, Part C, Geological Survey of Canada, Paper 76-1C: 191-193.

Hurford, A.J., and Green, P.F. 1983. The zeta age calibration of fission-track dating. Isotope Geoscience, **1**: 285-317.

Jochum, K.-P., and Stoll, B. 2008. Reference materials for elemental and isotopic analysis by LA-(MC)-ICP-MS: Successes and outstanding needs. *In* Laser ablation-ICP-MS in the earth sciences, current practices and outstanding issues. *Edited by* P. Sylvester. Mineralogical Association of Canada (MAC) Short Course Series, Vancouver. pp. 147-168.

Le Maitre, R.W., Streckeisen, A., Zanettin, B., Le Bas, M.J., Bonin, B., Bateman, P., Bellieni, G., Dudek, A., Efremova, A., and Keller, J. 2002. Igneous rocks. a classification and glossary of terms. Recommendations of the IUGS Subcommission on the Systematics of Igneous Rocks. Cambridge University Press, Cambridge.

Lindsey, D.A., Naeser, C.W., and Shawe, D.R. 1975. Age of volcanism, intrusion and mineralization in the Thomas Range, Keg Mountains, and Desert Mountain, western Utah. United States Geological Survey, Journal of Research, **3:** 597-604.

Lowdon, J.A., and Blake, W., Jr. 1975. Geological Survey of Canada radiocarbon dates XV. Geological Survey of Canada, Paper 75-7, 32 p.

Mark, D.F., Renne, P.R., Dymock, R.C., Smith, V.C., Simon, J.I., Morgan, L.E., Staff, R.E., Ellis, B.S., and Pearce, N.J.G. 2017. High-precision $^{40}Ar/^{39}Ar$ dating of Pleistocene tuffs and temporal anchoring of the Matuyama – Brunhes boundary. Quaternary Geochronology, **39**: 1-23.

Naeser, C.W., and Naeser, N.D. 1988. Fission-track dating of Quaternary events. *In* Dating Quaternary sediments. *Edited by* D.J. Easterbrook. Geological Society of America Special Paper, **227**: 1-11.

Naeser, N.D., Westgate, J.A., Hughes, O.L., and Péwé, T.L. 1982. Fission-track ages of late Cenozoic distal tephra beds in the Yukon Territory and Alaska. Canadian Journal of Earth Sciences, **19**: 2167-2178.

Pearce, J.A. 1982. Trace element characteristics of lavas from destructive plate boundaries. *In* Andesites: Orogenic andesites and related rocks. *Edited by* R.S.Thorpe. Wiley, Chichester. pp. 526–547.

Pearce, J.A., Harris, N.B., and Tindle, A.G. 1984. Trace element discrimination diagrams for the tectonic interpretation of granitic rocks. Journal of Petrology, **25(4)**: 956-983.

Pearce, N.J.G. 2014. Towards a protocol for the analysis of rhyolitic glass shards in tephra deposits by laser ablation ICP-MS. Journal of Quaternary Science, **29**: 627-640.

Pearce, N.J.G., Perkins, W.T., Westgate, J.A., Gorton, M.P., Jackson, S.E., Neal, C.R., and Chenery, S.P. 1997. A compilation of new and published major and trace element data for NIST SRM 610 and NIST SRM 612 glass reference materials. Geostandards Newsletter, **21**: 115-144.

Pearce, N.J.G., Perkins, W.T., Westgate, J.A., and Wade, S.C. 2011. Trace element analysis by laser ablation ICP-MS: the quest for comprehensive chemical characterization of single sub-10μm volcanic glass shards. Quaternary International, **246**: 57-81.

Pearce, N.J.G., Abbott, P.M., and Martin-Jones, C. 2014. Microbeam methods for the analysis of glass in fine grained tephra deposits: a SMART perspective on current and future trends. *In*

Marine tephrochronology. *Edited by* W.E.N. Austin, P.M. Abbott, S.M. Davies, N.J.G. Pearce, and S. Wastegård. Geological Society Special Publications, **398**: 29-46.

Pillans, B., and Gibbard, P. 2012. The Quaternary Period. *In* The Geologic Time Scale 2012. *Edited by* F.M. Gradstein, J.G. Ogg, M. Schmitz, and G. Ogg. Elsevier, Amsterdam. pp. 979-1010.

Sandhu, A.S., and Westgate, J.A. 1995. The correlation between reduction in fission-track diameter and areal track density in volcanic glass shards and its application in dating tephra beds. Earth and Planetary Science Letters, **131**: 289-299.

Schmieder, M., Kennedy, T., Jourdan, F., Buchner, E., and Reimold, W.U. 2018. A high-precision $^{40}Ar/^{39}Ar$ age for the Nördlinger Ries impact crater, Germany, and implications for the accurate dating of terrestrial impact events. Geochemica et Cosmochimica Acta, **220**: 146-157.

Smith, D.G.W., and Westgate, J.A. 1968. Electron probe technique for characterising pyroclastic deposits. Earth and Planetary Science Letters, **5**: 313-319.

Stalker, A. MacS. 1977. The probable extent of Classical Wisconsin ice in southern and central Alberta. Canadian Journal of Earth Sciences, **14**: 2614-2619.

Stalker, A. MacS., and Churcher, C.S. 1972. Glacial stratigraphy of the southwestern Canadian prairies; the Laurentide record. *In* 24th International Geological Congress, Section 12: 110-119.

Sun, S.-s., and McDonough, W.F. 1989. Chemical and isotopic systematics of oceanic basalts: implications for mantle composition and processes. *In* Magmatism in the ocean basins.

Edited by A.D. Saunders and M.J. Norry. Geological Society Special Publications, **42**: 313-345.

Thompson, R.N., Dickin, A.P., Gibson, I.L., and Morrison, M.A. 1982. Elemental fingerprints of isotopic contamination of Hebridean Palaeocene mantle-derived magmas by Archaean sial. Contributions to Mineralogy and Petrology, **79**: 159-168.

Wagner, G.A., and Van den Haute, P. 1992. Fission-track dating. Kluwer, Stuttgart, Germany, 285 p.

Westgate, J.A. 1968. Surficial geology of the Foremost – Cypress Hills area, Alberta. Research Council of Alberta, Bulletin 22, 121 p.

Westgate, J.A. 2015. Volcanic glass (fission track). *In* Encyclopedia of scientific dating methods. *Edited by* W.J. Rink and J.W.Thompson. Springer, Dordrecht, The Netherlands. pp. 941-946.

Westgate, J.A., and Evans, M.E. 1978. Compositional variability of Glacier Peak tephra and its stratigraphic significance. Canadian Journal of Earth Sciences, **15**: 1554-1567.

Westgate, J.A., and Fulton, R.J., 1975. Tephrostratigraphy of the Olympia interglacial sediments in southern British Columbia, Canada. Canadian Journal of Earth Sciences, **12**: 489-502.

Westgate, J.A., Christiansen, E.A., and Boellstorff, J.D. 1977. Wascana Creek Ash (Middle Pleistocene) in southern Saskatchewan: characterization, source, fission track age, palaeomagnetism and stratigraphic significance. Canadian Journal of Earth Sciences, **14**: 357-374.

Westgate, J.A., Briggs, N.D., Stalker, A. MacS., and Churcher, C.S. 1978. Fission track age of glass from tephra beds associated with Quaternary vertebrate assemblages in the southern Canadian plains. Geological Society of America, Abstracts with Programs, **10**: 514-515.

Westgate, J.A., Walter, R.C., Pearce, G.W., and Gorton, M.P. 1985. Distribution, stratigraphy, petrochemistry and palaeomagnetism of the late Pleistocene Old Crow tephra in Alaska and the Yukon. Canadian Journal of Earth Sciences, **22**: 893-906.

Westgate, J.A., Pearce, N.J.G., Gatti, E., and Achyuthan, H. 2014. Distinction between the Youngest Toba Tuff and Oldest Toba Tuff from northern Sumatra based on the area density of spontaneous fission tracks in their glass shards. Quaternary Research, **82**: 388-393.

Westgate, J.A., WoldeGabriel, G., Halls, H.C., Bray, C.J., Barendregt, R.W., Pearce, N.J.G., Sarna-Wojcicki, A.M., Gorton, M.P., Kelley, R.E., and Schultz-Fellenz, E. 2019. Quaternary tephra from Valles caldera in the volcanic field of the Jemez Mountains of New Mexico identified in western Canada. Quaternary Research, **81**: 813-828.

Whitaker, S.H., and Christiansen, E.A. 1972. The Empress Group in southern Saskatchewan. Canadian Journal of Earth Sciences, **9**: 353-360.

Captions to Figures

Fig. 1. Location of Wellsch Valley tephra (UA115) in southwest Saskatchewan at 50° 39.92’N, 107° 52.5’W and Galt Island tephra (UA117) in southeast Alberta at 50° 4.67’N, 110° 49.38’W. The relevant part of a road map of western Canada was scanned using Epson Perfection V850 Pro and then copied into CorelDRAW Graphic Suite 2019, which was used to add the prominent geographic features, place names, and sample locations.

Fig. 2. Location and geomorphic setting of UA115 and UA117 tephra beds in the South Saskatchewan River Valley. Images modified from Google Earth Pro.

Fig. 3. Lithostratigraphic context of Wellsch Valley tephra based mostly on a written communication from Dr. A. Stalker, Geological Survey of Canada, in 1978, but augmented by observations in the field by JW that focused on the tephra bed and its immediately surrounding sediments. Sediments below the glacial deposits and above bedrock belong to the Empress Group.

Fig. 4. Wellsch Valley tephra (white bed), mostly reworked, with evidence of rodent burrows. Tephra fills cracks in the underlying sediments. Scale is in centimetres.

Fig. 5. Grain-size distributions of Wellsch Valley tephra (dots, n=4) and Galt Island tephra (crosses, n=1). The particle-size distribution of the sand fraction was determined using sieves and the finer-size fraction by use of the hydrometer method as specified in the ASTM D7928 procedure.

Fig. 6. Sketch of the lithostratigraphic context of Galt Island tephra based on a visit to the site with Dr. A. Stalker, Geological Survey of Canada, in 1978 as well as a written communication from him in that year. Thickness of units is approximate. The enlarged diagram of the basal part of the Quaternary sediments includes the Galt Island tephra (sampled horizon A), which occurs directly above a thin bed of preglacial gravels overlying Cretaceous bedrock. The paleomagnetic sampling horizons (A-O) embrace the lowermost ~20 m of the Quaternary sediments including the fine-grained fluvial sediments and the lower part of the overlying lacustrine silt and clay. Details on the ^{14}C ages are given in the text.

Fig. 7. Wellsch Valley tephra and Galt Island tephra are closely grouped with tephra derived from vents in the Cascade Range of the Pacific Northwest and are distinctive with respect to tephra of intraplate volcanism (e.g. Yellowstone volcanic field). Tephra from the following volcanoes in the Cascade Range were analyzed: Crater Lake in Oregon, Glacier Peak, Mt. St. Helens, and Mount Baker (Lake Tapps tephra) in Washington State, and Bridge River in southern British Columbia (Westgate et al. 2019). Tephra beds in the Olympia interglacial sediments are most likely derived from Mt. St. Helens (Westgate and Fulton 1975). Tephra samples from intraplate volcanism come from volcanic fields along the Yellowstone Hotspot Track and the Valles caldera in New Mexico. The composition of glass shards of tephra from the Long Valley caldera in California is not presented here but they would plot close to the group of intraplate volcanics having much lower concentrations of CaO than tephra from volcanoes in the Cascade Range (Westgate et al. 2019).

Fig. 8. Selected trace element data from individual glass shards in WVt and Gt. Bivariate plots show a range of compatible and incompatible elements, with differences in composition evident between the two tephra beds. **Below left:** Chondrite-normalized incompatible element spidergram for glass shards of WVt UA115 (n = 19) and Gt UA117 (n = 16) using average values for element concentrations. Sharp depletions at Sr, and Ti result from fractionation of plagioclase, and Fe-Ti oxides. The pronounced Nb – Ta trough is a feature of parental magmas which originated in a continental-margin subduction environment. Normalization factors from Thompson et al. (1982). **Below right:** Chondrite-normalized REE diagram for glass shards of WVt UA115 (n = 19) and Gt UA117 (n = 16) using average values for element concentrations. Chondrite REE concentrations from Sun and McDonough (1989). All trace element concentrations in ppm.

Fig. 9. Changes in remanent magnetization directions (inclination only) following 5 mT alternating field demagnetization (A) from 1978 data (previously unpublished), and (B) following 10, 30, 50, and 70 mT alternating field demagnetization from Barendregt (1984) data. Both studies reveal inclination profiles indicating a change from reversed to normal polarity at the top of the WVt (0.75 ± 0.05 Ma) and based on the most recent age reported for the Brunhes/Matuyama Chron boundary (783.4 ± 0.6 ka), the polarity reversal occurred soon after deposition of the WVt (Table 3). Locality B is 15 m east of locality A. Sediments at and below WVt belong to the Empress Group.

Fig. 10. Inclination and declination profiles for sediments at the Galt Island site, following 10, 30, 50, and 70 mT alternating field demagnetization. Remanence directions, magnetization, precision, and confidence limits are shown. All sediments, including the Galt Island tephra, are normally magnetized, and, based on the age of Galt Island tephra (0.49 ± 0.05 Ma), these sediments, including the tephra, were deposited during the early Brunhes Chron. Explanation of symbols: *n*, number of specimens in each of the sampled horizons (A-O, Fig. 6); *D* and *I*, declination and inclination, respectively, (°); *M*, intensity of magnetization of the mean direction, (mA/m); *k*, precision parameter; α_{95}, circle of confidence (P = 0.05). The mean inclination expected for a geocentric axial dipole at this latitude is 67.8°. Galt Island tephra (UA117) is at horizon A (Fig. 6).

Table 1. Average major- and trace-element composition of glass shards in Wellsch Valley tephra and Galt Island tephra, western Canada

	Wellsch Valley tephra	Galt Island tephra	Old Crow tephra	
Sample	UA115	UA117	UT1727	
			this study	reference values
wt%				
SiO_2	73.66 ± 0.46	75.97 ± 0.88	75.36 ± 0.20	75.42 ± 0.31
TiO_2	0.23 ± 0.11	0.26 ± 0.12	0.20 ± 0.08	0.30 ± 0.07
Al_2O_3	14.85 ± 0.19	13.21 ± 0.39	13.10 ± 0.15	13.08 ± 0.19
FeO_t	1.53 ± 0.10	1.34 ± 0.22	1.66 ± 0.06	1.72 ± 0.08
MnO	*0.07 ± 0.05*	*0.07 ± 0.04*	0.11 ± 0.08	0.07 ± 0.04
CaO	1.43 ± 0.09	1.40 ± 0.24	1.46 ± 0.08	1.50 ± 0.07
MgO	0.36 ± 0.04	0.30 ± 0.08	0.29 ± 0.03	0.28 ± 0.03
Na_2O	4.83 ± 0.34	4.15 ± 0.17	3.91 ± 0.13	3.73 ± 0.24
K_2O	2.94 ± 0.12	3.18 ± 0.21	3.63 ± 0.07	3.70 ± 0.13
Cl	0.12 ± 0.05	0.14 ± 0.04	0.29 ± 0.04	0.28 ± 0.04
H_2O_d	4.81 ± 0.56	4.55 ± 0.53	3.19 ± 0.83	4.93 ± 1.51
n=	30	17	10	542
			ATHO-G	
ppm			This study±1 s.d.	GeoReM±95% CL
Rb	66.3 ± 4.9	73.4 ± 4.0	66.6 ± 2.3	65.3 ± 3
Sr	302 ± 36	254 ± 63	95.2 ± 1.8	94.1 ± 2.7
Y	20.3 ± 1.7	21.1 ± 2.8	92.0 ± 2.7	94.5 ± 3.5
Zr	298 ± 33	207 ± 46	486 ± 9	512 ± 20
Nb	10.7 ± 1.5	9.17 ± 0.66	61.7 ± 1.7	62.4 ± 2.6
Cs	1.80 ± 0.26	1.93 ± 0.35	1.12 ± 0.10	1.08 ± 0.11
Ba	905 ± 93	973 ± 98	503 ± 13	547 ± 16
La	30.7 ± 3.6	30.4 ± 3.5	52.0 ± 0.8	55.6 ± 1.5
Ce	55.0 ± 4.8	53.4 ± 3.6	115 ± 3	121 ± 4
Pr	6.36 ± 0.77	6.24 ± 0.88	13.6 ± 0.2	14.6 ± 0.4
Nd	23.8 ± 2.6	23.1 ± 3.4	57.4 ± 2.8	60.9 ± 2
Sm	4.09 ± 0.70	5.00 ± 1.29	13.0 ± 1.6	14.2 ± 0.4
Eu	0.92 ± 0.19	0.87 ± 0.38	2.64 ± 0.2	2.76 ± 0.1
Gd	3.33 ± 0.82	4.87 ± 1.76	14.4 ± 1.1	15.3 ± 0.7
Tb	0.55 ± 0.10	0.70 ± 0.28	2.41 ± 0.10	2.51 ± 0.08
Dy	3.43 ± 0.59	3.84 ± 1.23	16.2 ± 0.8	16.20 ± 0.7
Ho	0.67 ± 0.17	0.65 ± 0.18	3.41 ± 0.19	3.43 ± 0.11
Er	2.36 ± 0.52	2.74 ± 0.81	10.6 ± 0.5	10.3 ± 0.5
Tm	0.40 ± 0.13	0.42 ± 0.13	1.47 ± 0.10	1.52 ± 0.07
Yb	2.89 ± 0.47	2.91 ± 0.73	9.84 ± 0.64	10.5 ± 0.4
Lu	0.49 ± 0.10	0.51 ± 0.19	1.53 ± 0.11	1.54 ± 0.05
Hf	7.91 ± 1.42	7.14 ± 1.10	13.5 ± 0.4	13.7 ± 0.5
Ta	1.06 ± 0.18	0.99 ± 0.27	3.77 ± 0.25	3.9 ± 0.2
Pb	27.8 ± 5.4	27.1 ± 5.5	6.03 ± 1.07	5.67 ± 0.62
Th	12.6 ± 1.4	15.0 ± 1.8	7.11 ± 0.34	7.4 ± 0.27
U	4.46 ± 0.51	5.04 ± 0.69	2.38 ± 0.10	2.37 ± 0.12
n=	19	16	5	

Notes: Major and minor elements recast to anhydrous analyses. FeO_t is total iron as FeO;
H_2O_d is water by difference. Details on instruments used and operating conditions are specified in the Methods section of the text. Analyses of individual glass shards are given in Tables S1, S2.
Averages for trace element compositions include outlying analyses.
See also supplementay tables of major and trace element data

Table 2 . Average major-element composition of FeTi oxides in Wellsch Valley tephra and Galt Island tephra

	UA115		UA117	
wt%	Magnetite	Ilmenite	Magnetite	Ilmenite
SiO_2	0.58	0.57	0.51	0.97
TiO_2	9.16	37.76	7.38	37.25
Al_2O_3	2.22	0.31	2.02	0.35
Fe_2O_3	46.86	27.34	50.77	27.85
FeO	37.59	31.32	35.71	30.94
MnO	0.2	0.17	0.14	0.13
MgO	1.59	1.8	1.69	2.05
Total	98.2	99.26	98.22	99.54
n	23	9	17	10

Notes: Analyses done on an ARL "EMX" microprobe using the Ødergarden ilmenite and Elba hematite as standards. Total iron split into FeO and Fe_2O_3 using the method of Carmichael (1967). n is number of grains analyzed.

Table 3. Glass fission-track ages of Wellsch Valley tephra and Galt Island tephra

Sample number	Size fraction (mm)	Method for correction of partial track fading	ρ_s ($\times 10^2$ t/cm^2)	Corrected ρ_s ($\times 10^2$ t/cm^2)	ρ_i ($\times 10^4$ t/cm^2)	ρ_d ($\times 10^5$ t/cm^2)	Etching conditions for glass HF:temp:time (%: °C: s)	D_s (µm)	D_i (µm)	D_i / D_s	Age (Ma ± 1σ)
Wellsch Valley tephra											
UA115	0.125-0.088	DCFT	5.32 ± 0.80 (44)	6.71 ± 1.01 (44)	10.10 ± 0.20 (2595)	4.08 ± 0.04 (8233)	24: 22: 60	3.84 ± 0.29 [28]	4.84 ± 0.15 [57]	1.26 ± 0.10	0.85 ± 0.13
UA115	0.088-0.074	DCFT	3.59 ± 0.27 (173)	4.52 ± 0.34 (173)	8.09 ± 0.13 (3802)	4.08 ± 0.04 (8233)	24: 22: 60	3.84 ± 0.29 [28]	4.84 ± 0.15 [57]	1.26 ± 0.10	0.72 ± 0.06
UA115	0.088-0.074	1 hour at 200°C	n/a	3.28 ± 0.35 (88)	5.63 ± 0.10 (3305)	4.08 ± 0.04 (8233)	24: 23: 40	nd	nd	nd	0.75 ± 0.08
									Weighted mean age		**0.75 ± 0.05**
Galt Island tephra											
UA117	0.088-0.063	DCFT	1.67 ± 0.21 (61)	2.03 ± 0.26 (61)	6.44 ± 0.15 (1806)	4.83 ± 0.04 (9617)	24: 23: 60	nd	nd	1.22 ±0.04	0.48 ± 0.06
UA117	0.088-0.063	DCFT	1.80 ± 0.27 (45)	2.19 ± 0.33 (45)	6.47 ± 0.17 (1498)	4.83 ± 0.05 (9617)	24: 23: 60	nd	nd	1.22 ± 0.04	0.52 ± 0.08
									Weighted mean age		**0.49 ± 0.05**
Age reference standard											
Moldavite		n/a	123.0 ± 6.7 (341)	n/a	12.9 ± 0.28 (2067)	4.88 ± 0.05 (9617)	nr	n/a	n/a	n/a	14.6 ± 0.9

Notes: Glass shards dated by population-subtraction method; details are given in Westgate (2015).

Ages calculated using the fission-track age equation of Hurford and Green (1983), using the following values: $\lambda_D = 1.551 \times 10^{-10}$ yr^{-1}; g = 1; zeta (NDN) = 315 ± 3, determined by using NIST standard glass SRM 963 (Carpenter and Reimer 1974) and the Moldavite tektite glass age standard with an $^{40}Ar/^{39}Ar$ plateau age of 14.808 ± 0.021 Ma (2σ) (Schmieder et al. 2018). Uncertainty on fission-track age calculated by combining the Poisson errors on the spontaneous counts, the induced counts, and the counts in the muscovite detector covering NIST SRM 963 (Lindsey et al. 1975).

ρ_s, spontaneous track density; ρ_i, induced track density; D_s, mean spontaneous track diameter; D_i, mean induced track diameter; DCFT, diameter correction method (Sandhu and Westgate 1995); n/a, not applicable; nd, not determined; nr, not recorded. Number in parentheses is number of tracks counted. Number in square brackets is number of track diameters measured.

ρ_d, track density in muscovite detector covering National Institutes of Standards and Technology (NIST) standard glass SRM 963 (Carpenter and Reimer 1974); listed value was calculated by interpolation between values determined for standards placed at the top and bottom of the irradiation tube.

Age of Galt Island tephra corrected using an average D_i/D_s value (1.218 ± 0.04) from 50 determinations on glass shards from 38 different Cenozoic tephra beds (Westgate et al. 2014).

Table 4. Declination and inclination of remanent magnetization for Wellsch Valley tephra with respect to demagnetization level

Demagnetization level (mT)	1 cm above base of tephra		10 cm above base of tephra	
	Declination (°)	Inclination (°)	Declination (°)	Inclination (°)
NRM	70.2	-29.8	83.1	-9.5
5	67.1	-53.5	67.3	-21.3
10	65.0	-52.9	43.1	-35.2
15	68.5	-55.1	37.6	-55.1
20	69.8	-50.9	50.8	-48.3
25	62.6	-52.2	40.2	-34.7
30	64.6	-54.9	10.5	-47.7
40	62.7	-46.5	56.6	-63.3

Notes: NRM is the natural remanent magnetization.

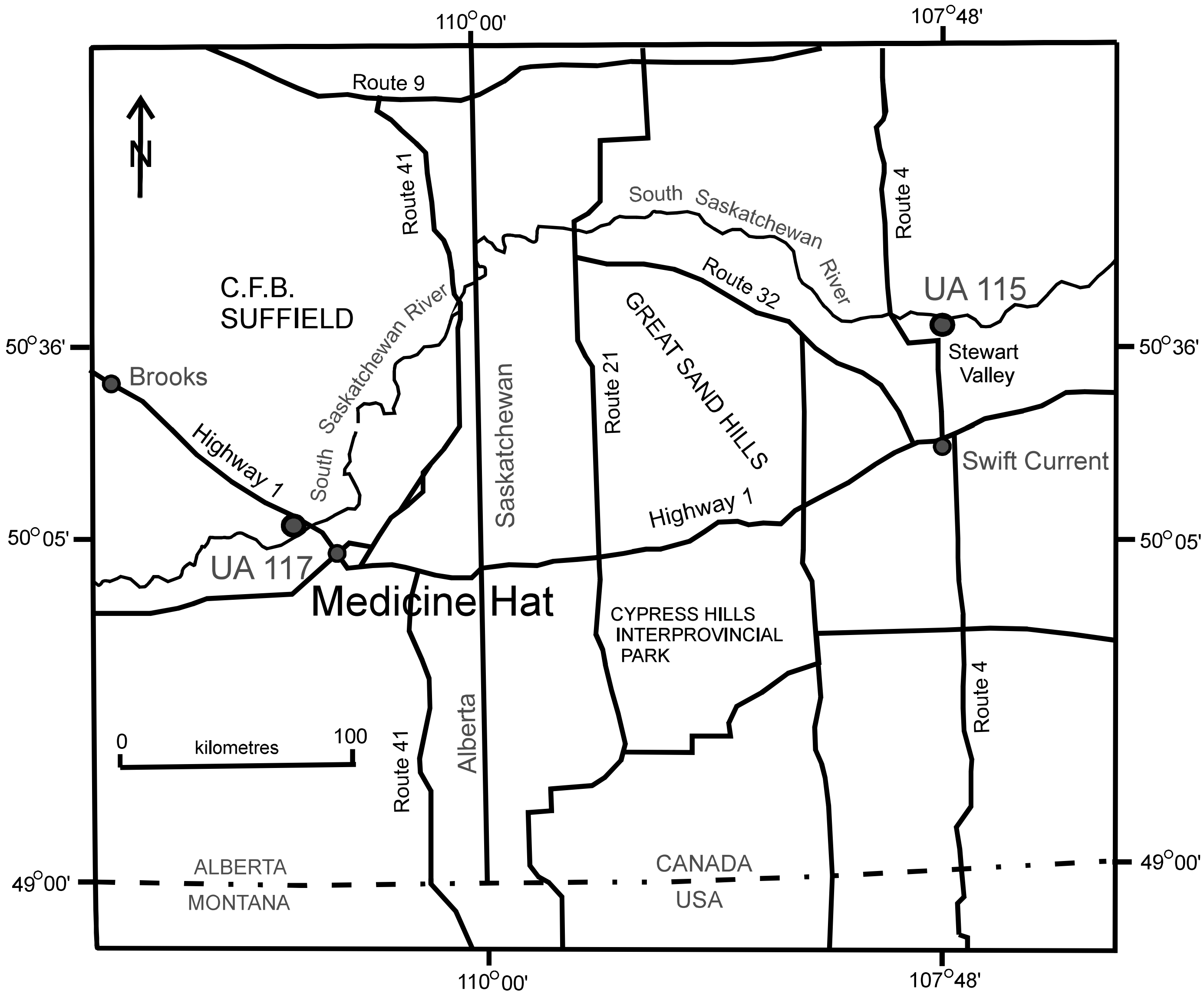
110°00'
107°48'
Route 9
N
Route 41
Route 4
South Saskatchewan River
C.F.B.
SUFFIELD
Route 32
GREAT SAND HILLS
UA 115
Stewart
Valley
50°36'
Brooks
Highway 1
South Saskatchewan River
Saskatchewan
Route 21
Swift Current
Highway 1
50°05'
UA 117
Medicine Hat
CYPRESS HILLS
INTERPROVINCIAL
PARK
0
kilometres
100
Route 41
Alberta
Route 4
ALBERTA
MONTANA
CANADA
USA
49°00'
110°00'
107°48'


Lake Diefenbaker
South Saskatchewan River Valley
UA 115
Saskatchewan Landing
Google Earth
N
5 km


UA 117
Redcliff
Google Earth
N
1 mi

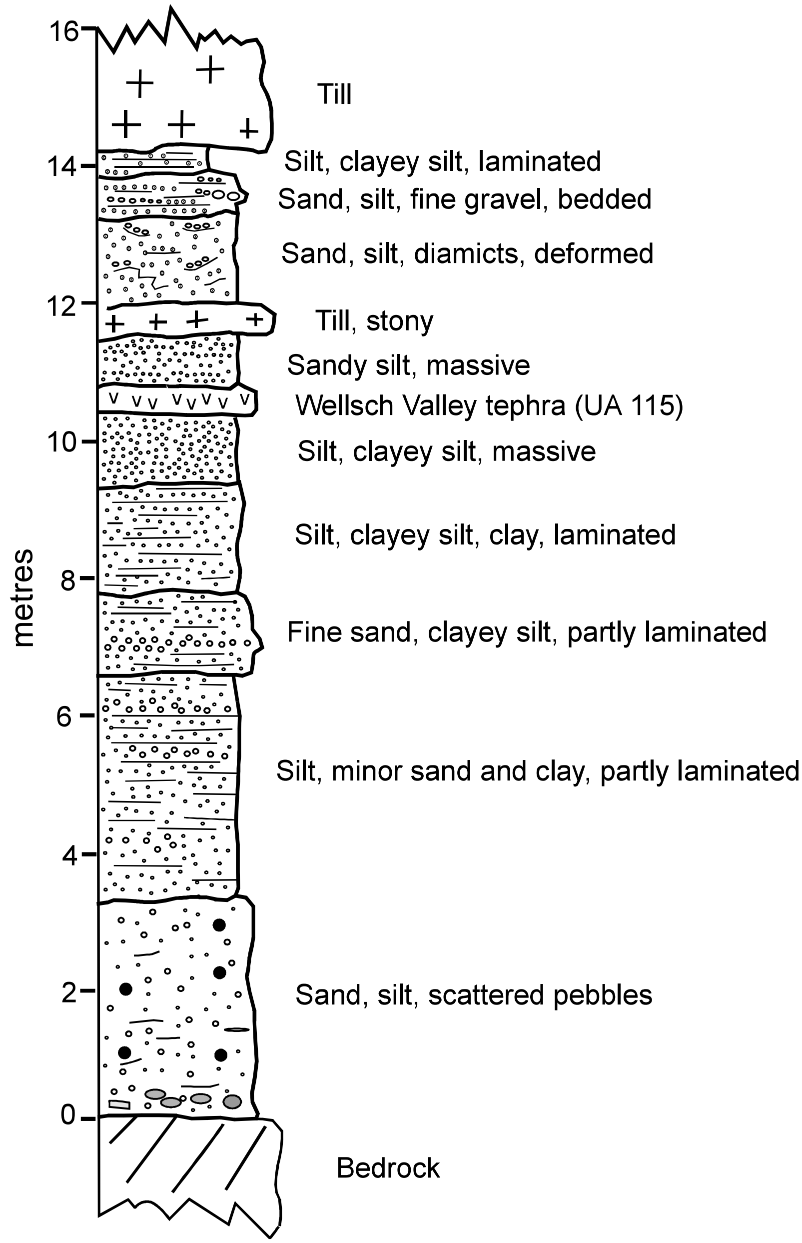
16
14
12
10
8
6
4
2
0
metres
Till
Silt, clayey silt, laminated
Sand, silt, fine gravel, bedded
Sand, silt, diamicts, deformed
Till, stony
Sandy silt, massive
Wellsch Valley tephra (UA 115)
Silt, clayey silt, massive
Silt, clayey silt, clay, laminated
Fine sand, clayey silt, partly laminated
Silt, minor sand and clay, partly laminated
Sand, silt, scattered pebbles
Bedrock

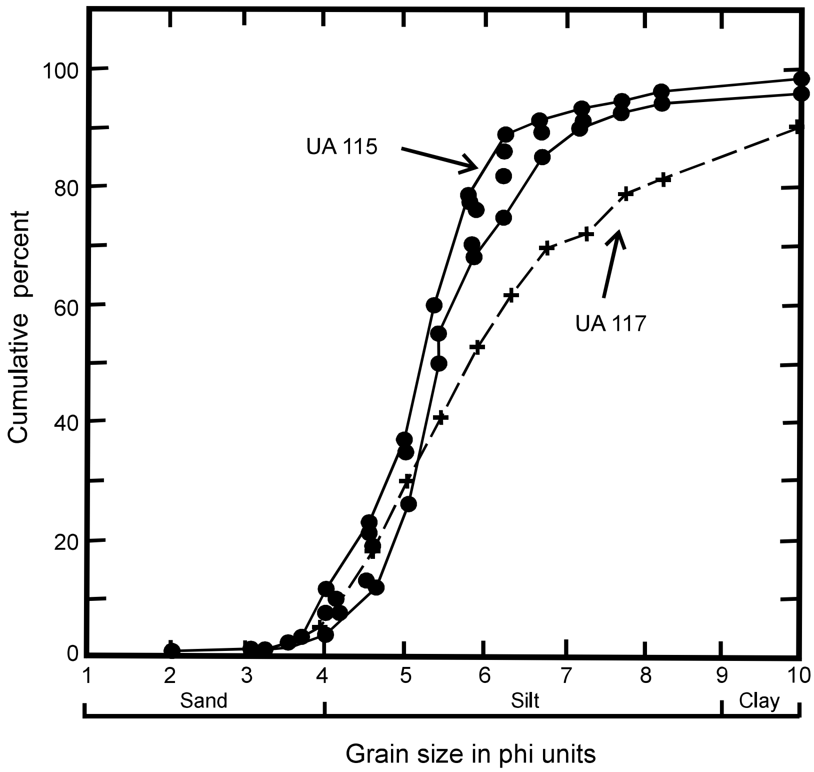
UA 115
UA 117
Cumulative percent
0
20
40
60
80
100
1
2
3
4
5
6
7
8
9
10
Sand
Silt
Clay
Grain size in phi units

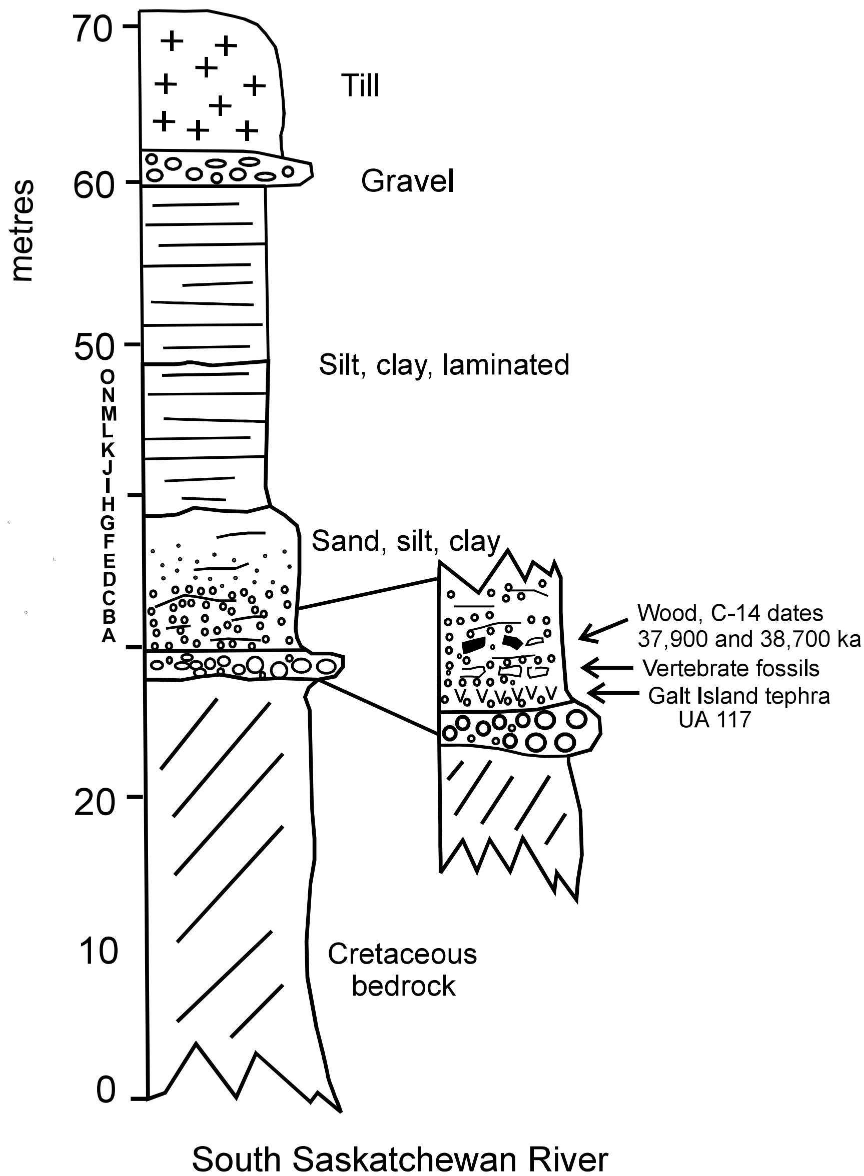
70
60
50
20
10
0
metres
O
N
M
L
K
J
I
H
G
F
E
D
C
B
A
Till
Gravel
Silt, clay, laminated
Sand, silt, clay
Wood, C-14 dates
37,900 and 38,700 ka
Vertebrate fossils
Galt Island tephra
UA 117
Cretaceous
bedrock
South Saskatchewan River

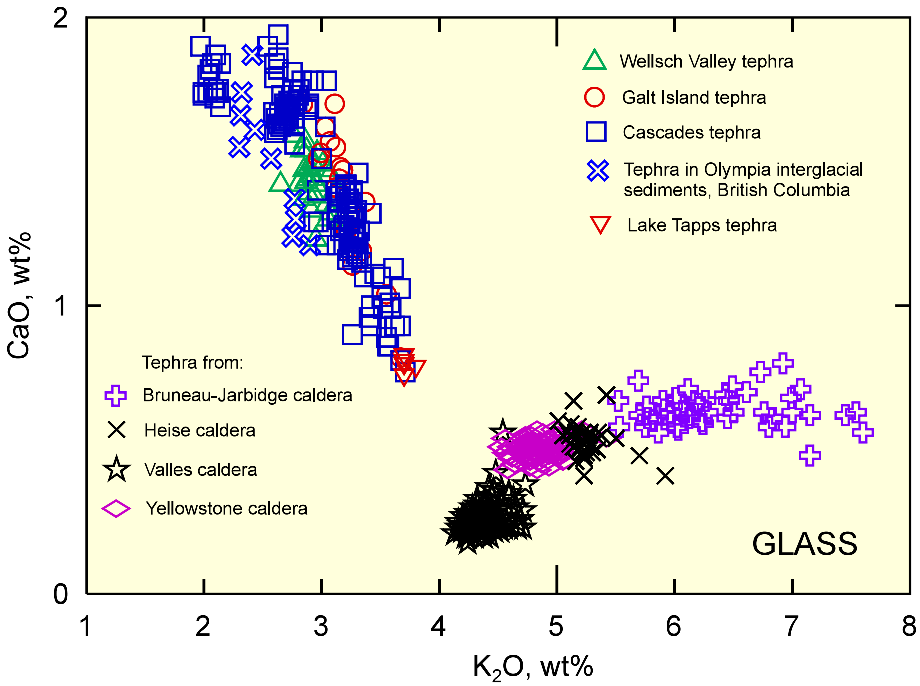
Wellsch Valley tephra
Galt Island tephra
Cascades tephra
Tephra in Olympia interglacial sediments, British Columbia
Lake Tapps tephra
Tephra from:
Bruneau-Jarbidge caldera
Heise caldera
Valles caldera
Yellowstone caldera
GLASS
CaO, wt%
K2O, wt%
0
1
2
1
2
3
4
5
6
7
8

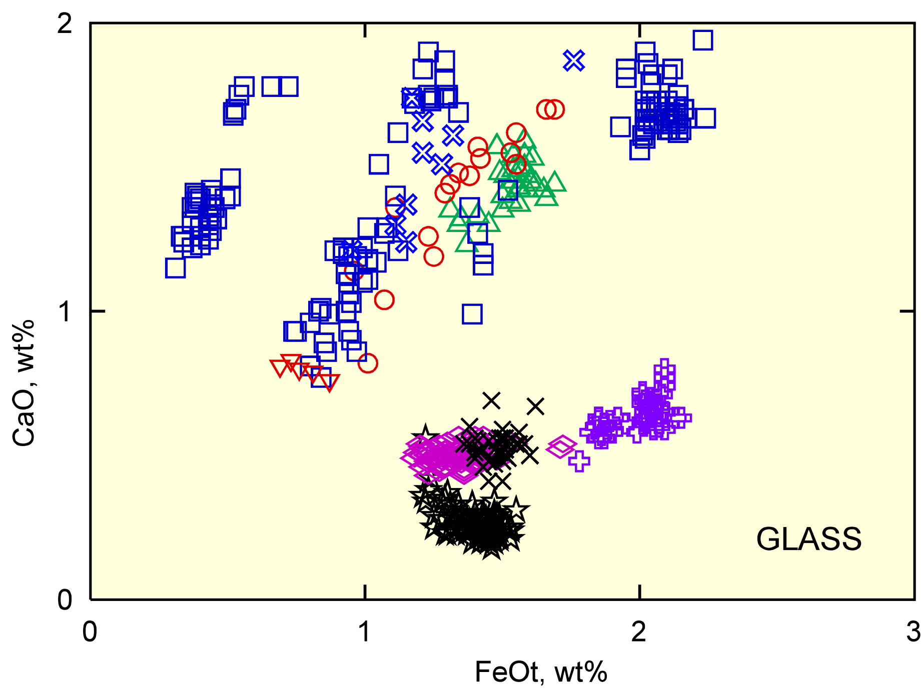
GLASS
CaO, wt%
FeOt, wt%
0
1
2
0
1
2
3

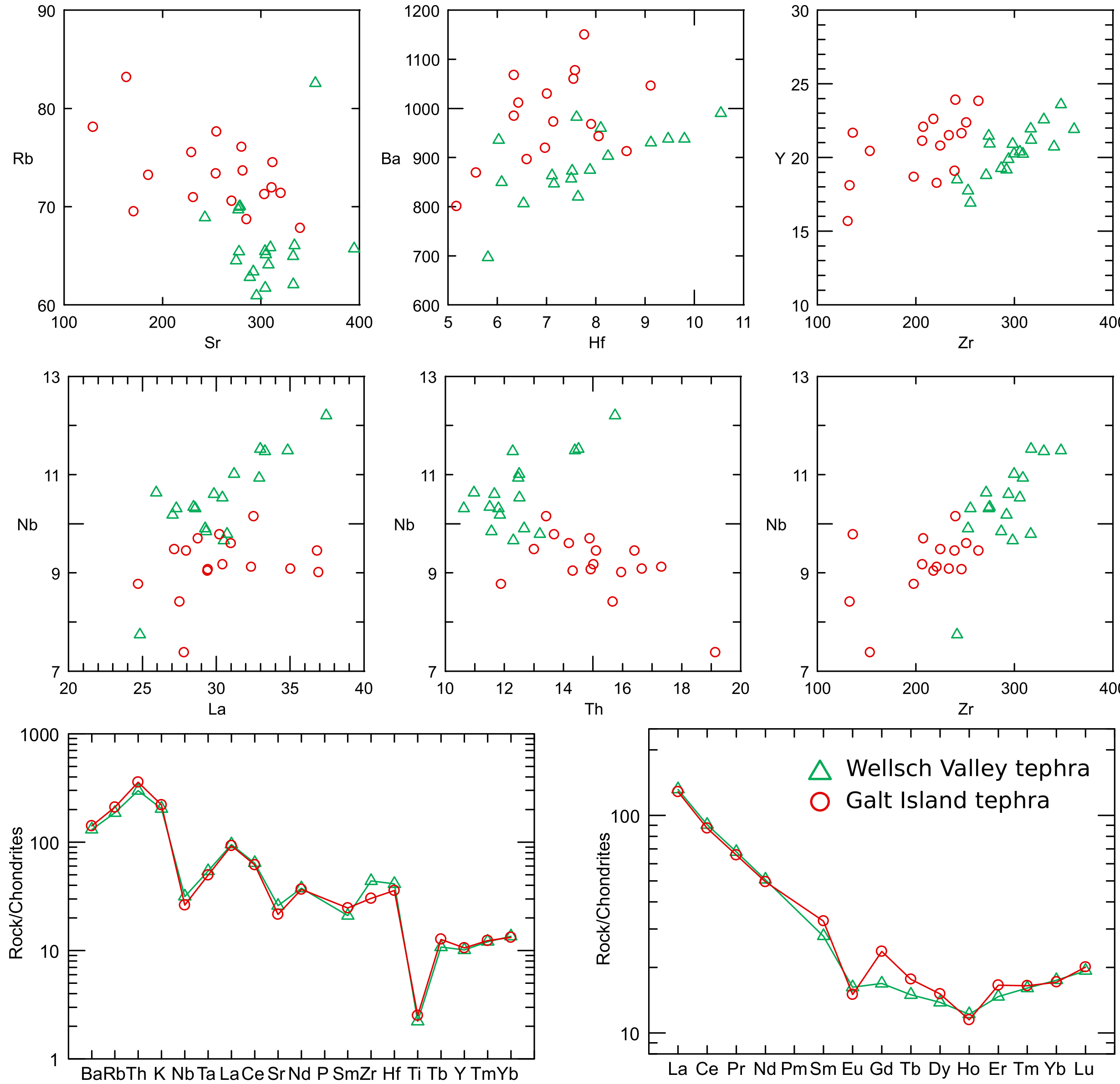
Rb
Sr
Ba
Hf
Y
Zr
Nb
La
Nb
Th
Nb
Zr
Rock/Chondrites
Ba Rb Th K Nb Ta La Ce Sr Nd P Sm Zr Hf Ti Tb Y Tm Yb
Rock/Chondrites
La Ce Pr Nd Pm Sm Eu Gd Tb Dy Ho Er Tm Yb Lu
Wellsch Valley tephra
Galt Island tephra

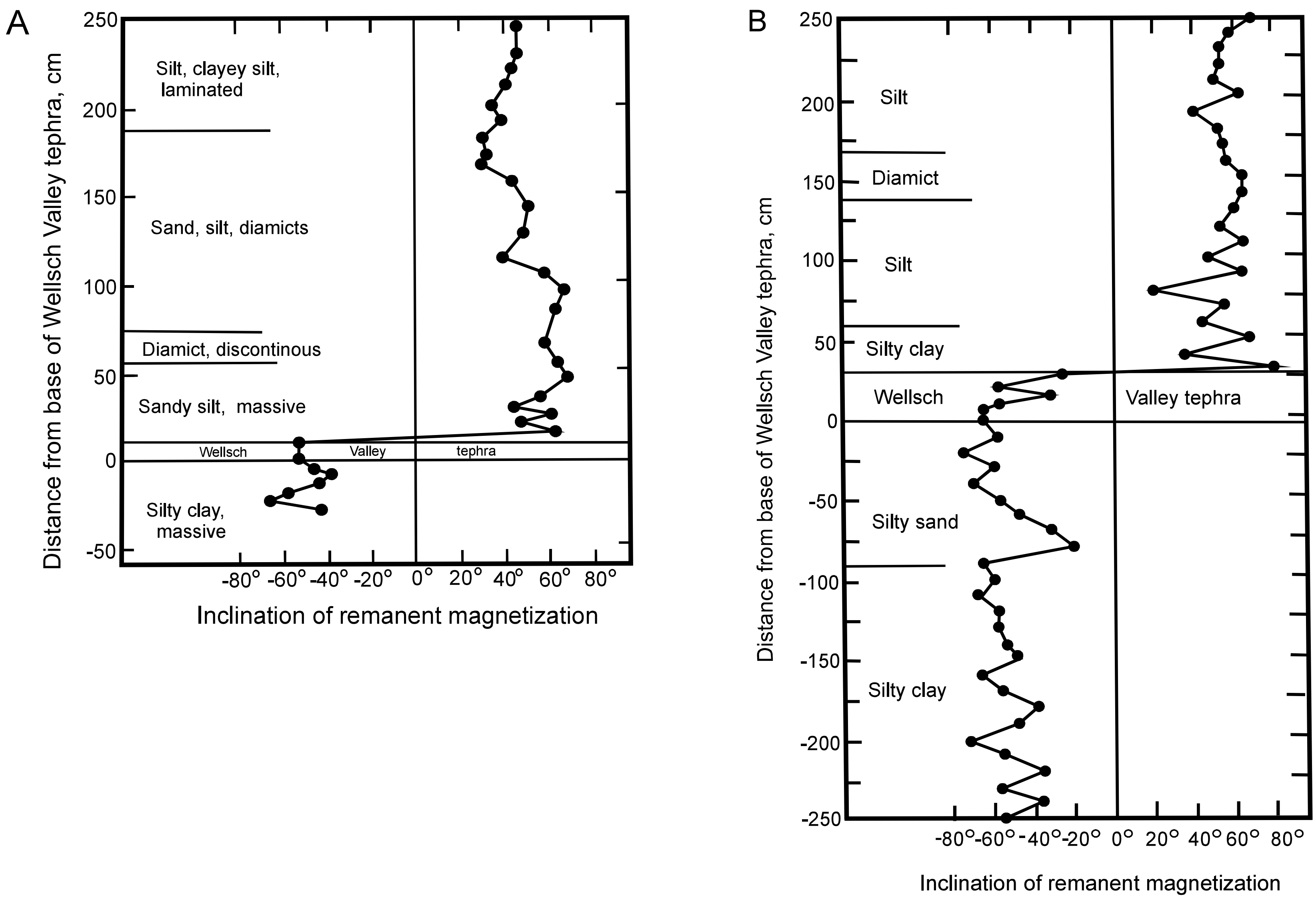
A
Distance from base of Wellsch Valley tephra, cm
250
200
150
100
50
0
-50
Silt, clayey silt, laminated
Sand, silt, diamicts
Diamict, discontinous
Sandy silt, massive
Wellsch
Valley
tephra
Silty clay, massive
-80° -60° -40° -20° 0° 20° 40° 60° 80°
Inclination of remanent magnetization
B
Distance from base of Wellsch Valley tephra, cm
250
200
150
100
50
0
-50
-100
-150
-200
-250
Silt
Diamict
Silt
Silty clay
Wellsch
Valley tephra
Silty sand
Silty clay
-80° -60° -40° -20° 0° 20° 40° 60° 80°
Inclination of remanent magnetization

Lithology	Site	*n*	*I*	*D*	*M*	*k*	α_{95}
Laminated silt and clay	O	8	43	325	4	36	3
	N	8	32	313	17	40	3
	M	8	45	321	15	21	18
	L	8	57	47	46	28	6
	K	8	51	1	10	123	6
	J	8	28	357	21	19	16
	I	8	2	329	8	85	7
	H	8	15	332	24	51	8
Clay	G	8	40	350	17	101	6
	F	8	48	354	20	83	6
Silt	E	8	70	10	13	66	8
	D	8	66	349	11	158	4
Fine sand	C	8	63	354	15	54	8
	B	8	69	28	18	50	8
Tephra	A	8	70	10	18	105	6